Surface Science 650 (2016) 149–160

Contents lists available at ScienceDirect

Surface Science

journal homepage: www.elsevier.com/locate/susc

Adsorption of isophorone and trimethyl-cyclohexanone on Pd(111): A combination of infrared reflection absorption spectroscopy and density functional theory studies

Karl-Heinz Dostert [a], Casey P. O'Brien [a], Wei Liu [a,c], Wiebke Riedel [a], Aditya Savara [a], Alexandre Tkatchenko [a], Swetlana Schauermann [a,b,*], Hans-Joachim Freund [a]

[a] Fritz-Haber-Institut der Max-anck-Gesellschaft, Faradayweg 4-6, 14195 Berlin, Germany
[b] Institut für Physikalische Chemie, Christian-Albrechts-Universität zu Kiel, Max-Eyth-Str. 2, 24118 Kiel, Germany
[c] Nano Structural Materials Center, School of Materials Science and Engineering, Nanjing University of Science and Technology, Nanjing 210094, Jiangsu, China

ARTICLE INFO

Available online 4 February 2016

Keywords:
Infrared spectroscopy
Density functional calculations
Palladium
Isophorone
Trimethylcyclohexanone

ABSTRACT

Understanding the interaction of α,β-unsaturated carbonyl compounds with late transition metals is a key prerequisite for rational design of new catalysts with desired selectivity towards C = C or C = O bond hydrogenation. The interaction of the α,β-unsaturated ketone isophorone and the saturated ketone TMCH (3,3,5-trimethylcyclohexanone) with Pd(111) was investigated in this study as a prototypical system. Infrared reflection–absorption spectroscopy (IRAS) and density functional theory calculations including van der Waals interactions (DFT + vdW^{surf}) were combined to form detailed assignments of IR vibrational modes in the range from 3000 cm^{-1} to 1000 cm^{-1} in order to obtain information on the binding of isophorone and TMCH to Pd(111) as well as to study the effect of co-adsorbed hydrogen. IRAS measurements were performed with deuterium-labeled (d_5-) isophorone, in addition to unlabeled isophorone and unlabeled TMCH. Experimentally observed IR absorption features and calculated vibrational frequencies indicate that isophorone and TMCH molecules in multilayers have a mostly unperturbed structure with random orientation. At sub-monolayer coverages, strong perturbation and preferred orientations of the adsorbates were found. At low coverage, isophorone interacts strongly with Pd(111) and adsorbs in a flat-lying geometry with the C = C and C = O bonds parallel, and a CH_3 group perpendicular, to the surface. At intermediate sub-monolayer coverage, the C = C bond is strongly tilted, while the C = O bond remains flat-lying, which indicates a prominent perturbation of the conjugated π system. Pre-adsorbed hydrogen leads to significant changes in the adsorption geometry of isophorone, which suggests a weakening of its binding to Pd(111). At low coverage, the structure of the CH_3 groups seems to be mostly unperturbed on the hydrogen pre-covered surface. With increasing coverage, a conservation of the in-plane geometry of the conjugated π system was observed in the presence of hydrogen. In contrast to isophorone, TMCH adsorbs in a strongly tilted geometry independent of the surface coverage. At low coverage, an adsorbate with a strongly distorted C = O bond is formed. With increasing exposure, species with a less perturbed C = O group appear.

1. Introduction

Chemo- and enantioselectivity in hydrogenation of α,β-unsaturated carbonyls on transition metals is a widely discussed topic in the field of heterogeneous catalysis. Particularly important is the possibility to control the selective hydrogenation of α,β-unsaturated ketones and aldehydes, which represent a broad class of valuable intermediates for practically important processes [1–3]. For molecules containing both a C = C and a C = O π-bond, such as the α,β-unsaturated ketone isophorone (3,5,5-trimethylcyclohex-2-enone), hydrogenation can yield either a saturated ketone, an unsaturated alcohol or a saturated alcohol. To avoid the formation of undesired products and thereby an often difficult and costly separation of the different products, a high selectivity towards hydrogenation of either the C = C or C = O bonds is desirable. Over Pd catalysts, the hydrogenation of the C = C bond of isophorone is strongly favored, yielding the saturated ketone TMCH (3,3,5-trimethylcyclohexanone) in high selectivity (≈100%) and almost no alcohols [4–6]. The origin of this chemoselectivity is, however, not fully understood.

* Corresponding author at: Fritz-Haber-Institut der Max-anck-Gesellschaft, Faradayweg 4-6, 14195 Berlin, Germany.
E-mail address: schauermann@fhi-berlin.mpg.de (S. Schauermann).

http://dx.doi.org/10.1016/j.susc.2016.01.026

Not only a high chemoselectivity, but even a high enantioselectivity in hydrogenation reactions can be achieved over heterogeneous catalysts using chiral modifiers [7–10]. Compared to homogeneous catalysts traditionally applied for enantioselective reactions, the use of heterogeneous catalysts has operational, economical and often environmental advantages, so that heterogeneously catalyzed enantioselective hydrogenation has been recognized as a promising field of research. A number of different modifiers have been tested for the enantioselective hydrogenation of isophorone, which is a model compound for enantioselective hydrogenation of enones [7,11–18]. Although the origin of the enantioselective hydrogenation of isophorone is not well understood, Lambert et al. [19,20] have proposed a mechanism in which the stereochemistry of the chiral modifier and the adsorption geometry of isophorone on the Pd catalyst play a decisive role. More specifically, strong tilting of the unsaturated bonds on Pd was put forward to explain the enantioselective interaction of isophorone with the chiral modifier. To the best of our knowledge, the effects of isophorone coverage and co-adsorbed hydrogen on the isophorone adsorption geometry have not been investigated so far in surface science studies.

In our previous work we found that isophorone adsorbs in a flat-lying geometry with the C = C and C = O bonds parallel to the Pd(111) surface at low coverage [21,22]. Coverage dependent NEXAFS studies showed that the angles of both unsaturated bonds with respect to the surface increased with increasing isophorone coverage. The tilting is considerably more pronounced for the C = C bond, indicating a perturbation and strong structural distortion of the conjugated π system [22].

In this work, infrared reflection-absorption spectroscopy (IRAS) and density functional theory studies including van der Waals interactions (DFT + vdW^{surf} [23]) were used to assign vibrational modes of isophorone, d_5-isophorone, and TMCH as well as to study the effects of hydrogen co-adsorption. IRAS is a powerful tool not only for determining the vibrational frequencies of chemical bonds, but also – making use of the metal surface selection rule [24–26] – for probing their orientation with respect to the metal surface. Thus, the combination of IRAS studies at sub-monolayer coverages with DFT hold great potential to provide detailed insights into the interaction of isophorone and TMCH with Pd(111).

Our results show that IR absorption features of molecules at multilayer coverages agree well with the calculated vibrational frequencies for unperturbed molecules. At sub-monolayer coverages, isophorone is strongly perturbed by interacting with the Pd(111) surface. Both the C = C and C = O bonds are oriented parallel to the surface and the CH_3 groups are oriented perpendicular to the surface. Strong perturbations of the isophorone molecule are observed on pristine Pd(111), however, this effect is reduced by preadsorbing hydrogen on Pd(111). In contrast to isophorone, TMCH adsorbs on Pd(111) with a strongly tilted C = O bond at low coverages.

2. Experimental details and methods

IRAS experiments were performed at the Fritz-Haber-Institut, Berlin, in a UHV apparatus that has been described in detail before [27]. Isophorone, d_5-Isophorone, or TMCH were dosed onto the sample cooled to 120 K through a doubly differentially pumped multi-channel array source controlled by valves and shutters. The surface was precovered with hydrogen by dosing 100 L of H_2 through a second doubly differentially pumped multi-channel array source controlled by valves and shutters. The sources were operated at room temperature, and the beam diameter was chosen to exceed the sample size. The Pd(111) single crystal was cleaned prior to use by repeated cycles of Ar^+ ion bombardment at room temperature, annealing at 1000 K and oxidation in $1 \cdot 10^{-6}$ mbar O_2 at 750 K to remove residual carbon. The final cleaning cycle was stopped after annealing. The flatness and cleanliness of the Pd(111) single crystal surface were checked by low energy electron diffraction (LEED) and infrared reflection-absorption spectroscopy (IRAS) of adsorbed CO. IRAS data were acquired using a vacuum Fourier-Transform infrared (FT-IR) spectrometer (Bruker IFS 66v/S) with a spectral resolution of 2 cm^{-1} and using a mid-infrared (MIR) polarizer and p-polarized IR light. Isophorone (Acros Organics, 98%), d_5-isophorone (Quotient Bioresearch (Radiochemicals) Limited, 90%) and TMCH (Aldrich, 98%) were purified prior to the experiments by repeated freeze–pump–thaw cycles. The stated exposures for IRAS experiments are given in fractions of a monolayer (ML) that were determined by TPD experiments.

The DFT calculations were carried out using the PBE + vdW^{surf} method [28], as implemented in the FHI-aims all-electron code [29]. The PBE + vdW^{surf} method, which accurately and effectively include the vdW interactions and dielectric screening within the bulk, has been demonstrate to perform very well for both strongly and weakly bound adsorption systems [30–32]. The "tight" settings were employed for integration grids and standard numerical atom-centered orbitals basis sets in FHI-aims code. The scaled zeroth-order regular approximation [33] was used to treat relativistic effects for Pd atoms. We built up four-layer Pd slabs with a (4×4) unit cell, and each slab was separated by a 20 Å vacuum. The bottom two metal layers were constrained, whereas the uppermost two metal layers and the adsorbate were allowed to fully relax during geometry relaxations. For slab calculations, we used a $3 \times 3 \times 1$ k-points mesh. Based on the most stable geometries, infrared vibrational spectra were calculated by a second derivative of the energy from the numerical change of the forces arising from small finite displacements. Six finite displacements were applied to each of the atoms with a value of 0.005 Å. It should also be noted that our calculations were based on the harmonic approximations, while the experimental spectra were measured at 120 K. To scrutinize the feasibility of the calculated structures, we have also computed the *anharmonic* IR spectra for isophorone on Pd(111) using *ab initio* molecular dynamics simulations at 130 K. The simulations were run for up to 73 ps, and the calculated spectra on Pd(111) agree very well with the experimentally measured IR spectra showing a vanishing of C = O and C = C stretching modes as expected for a flat-lying isophorone [22].

For isophorone and TMCH molecules in gas phase, the infrared vibrational spectra were calculated based on the fully relaxed structures from the PBE + vdW method, as implemented in the FHI-aims code. In this code the infrared spectra were calculated by a second derivative of the energy from the numerical change of the forces arising from small finite displacements. Six finite displacements were applied to each of the atoms with a value of 0.005 Å.

3. Results and discussion

The adsorption of the unsaturated ketone isophorone (3,5,5-trimethylcyclohex-2-enon), deuterium substituted (d_5-) isophorone, and the saturated ketone TMCH (3,5,5-trimethylcyclohexanone) on Pd(111) at 120 K was studied under well-defined UHV conditions by infrared reflection-absorption spectroscopy (IRAS). IR vibrational frequencies were calculated by the DFT + vdW^{surf} method. The structural formulae of normal and d_5-isophorone are shown in Fig. 1a and b. In d_5-isophorone, the five hydrogen atoms attached to the C_6 ring are substituted by deuterium atoms, while the hydrogen atoms on the CH_3 groups were unlabeled. The structure of TMCH is shown in Fig. 1c). Molecular vibrations will be discussed according to the labeling of the ring positions and methyl groups as illustrated in Fig. 1. Ring positions are labeled with numbers 1 to 6, methyl groups are labeled with A, B, and C.

To the best our knowledge, no detailed assignment of IR vibrations of isophorone or TMCH is available in literature. Therefore, we compare our experimental and theoretical assignments of IR vibrations to those of the same functional groups in other molecules. Among a large number of IR studies on hydrocarbons with identical groups, we chose some of the most fundamental investigations [35–52] for comparison.

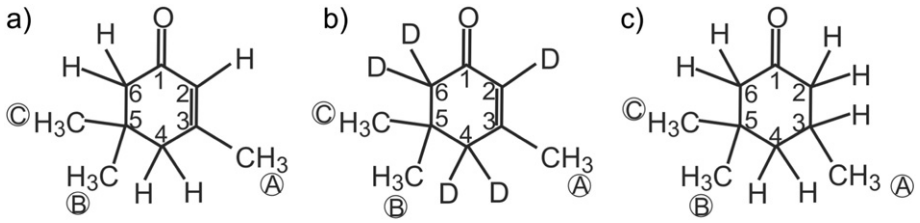

Fig. 1. Structures of the isophorone (a),d_5-isophorone (b)and TMCH (c).

We will briefly summarize only the most relevant results. An overview of typical vibrational frequencies of hydrocarbons can be found in a textbook by Colthup, Daly, and Wiberley [53]. In very early studies, Fox and Martin investigated CH_3, CH_2, and CH stretching vibrational modes from an experimental and theoretical point of view. The authors achieved a clear assignment of vibrational frequencies to CH_3, CH_2, and CH stretching modes in a large number of molecules. For instance, strong CH_3 stretching modes have been identified in several compounds near 2962 cm^{-1} and 2872 cm^{-1}. CH_2 stretching modes were typically observed near 2926 cm^{-1} and 2853 cm^{-1}. A CH stretching mode in olefins was assigned near 3019 cm^{-1}, while the CH vibration in saturated compounds was observed at 2890 cm^{-1} [35,36]. By using partially deuterium-labeled molecules, MacPhail et al. could distinguish CH_3 from CH_2 stretching modes in *n*-alkyl chains [38]. Studies on stretching modes of deuterium-labeled CD_2 groups are relatively rare. Nolin and Jones studied the IR absorption of normal and deuterium-substituted diethyl ketone. The authors assign CH_3 and CH_2 stretching and deformation vibrations as well as CD_3, CD_2 and C = O stretching modes. CH_3 asymmetric stretching appeared at 2977 cm^{-1} and 2936 cm^{-1}, while the symmetric stretching was observed at 2883 cm^{-1}. A CH_2 stretching mode was identified at 2902 cm^{-1} and CD_2 stretching at 2173 cm^{-1}. Moreover, the carbonyl (C = O) stretching mode was observed at 1720 cm^{-1}. CH_3 asymmetric bending modes were assigned at 1461 cm^{-1} and 1454 cm^{-1} and the symmetric bending mode was observed at 1379 cm^{-1}. The scissor vibrational mode of the CH_2 group was identified at 1414 cm^{-1} and thus, at relatively low frequency. This is of particular interest for our study, since in both cases the CH_2 groups are located next to a C = O group [45]. More general, Snyder and Schachtschneider presented very extensive interpretations of IR spectra of *n*-alkanes at 3000–2800 cm^{-1} and 1500–700 cm^{-1} in an experimental [40] and a theoretical [39] study. Lavalley and Sheppard investigated IR absorption features in the C–H stretching region, which result from Fermi resonance between CH_3 asymmetric deformation overtones and CH_3 symmetric stretching fundamentals [52]. A detailed study on the vibrational modes of linear and branched aliphatic hydrocarbons in the range below 1500 cm^{-1} was published by Sheppard et al. Some characteristic features were observed for non-linear molecules, such as a splitting of the CH_3 symmetric deformation into two bands for two CH_3 groups attached to the same saturated C atom [37]. Colthup found that this splitting is the result of an interaction force between two or three neighboring CH_3 groups. The same study shows that the exact wavenumber of CH_3, CH_2, and CH deformation vibrations is in general determined by the electron density at the respective C atom [41]. These references, along with DFT calculations from this work, form the basis for our assignment of infrared vibrational modes of isophorone and TMCH adsorbed on Pd(111).

In the following sections, we will first discuss the IR spectra of molecules in multilayers before focusing on coverage-dependent IR vibrations from multilayer to sub-monolayer coverage, where the interaction with the underlying palladium substrate becomes more important. Finally, the sub-monolayer structures of isophorone and TMCH will be compared. The comparison of the binding properties of isophorone and TMCH is of particular interest for catalysis, since hydrogenation of the C = C bond in isophorone yields TMCH.

3.1. IR vibrations in isophorone multilayers

In this section, we briefly discuss the IR spectra of multilayer-coverages of isophorone and d_5-isophorone on Pd(111). A more detailed assignment of molecular vibrations can be found in SI. The spectra are dominated by molecules organized in an ice structure, providing a reference for mainly non-perturbed molecules. DFT + vdW^{surf} calculations were performed for non-perturbed molecules in the gas-phase. Fig. 2 displays the IR spectra of 3 ML of isophorone and d_5-isophorone on Pd(111) at 120 K. For both molecules, three main spectral regions can be distinguished: C–H stretching (3200–2800 cm^{-1}), C = C and C = O stretching (1850–1550 cm^{-1}), and C–H, C–D and C–C deformation (<1500 cm^{-1}). C–D stretching vibrations (2300–2000 cm^{-1}) in d_5-isophorone are not shown in Fig. 2.

The DFT-calculated vibrational frequencies agree well with those observed experimentally in the C = O stretching region, but the DFT-calculated IR spectrum was scaled by a factor of 0.945 with the origin at 1661 cm^{-1} in order to compare the calculated vibrational frequencies to those observed experimentally in the 3100 cm^{-1} to 1000 cm^{-1} range. It has been observed before that calculated harmonic vibrational frequencies systematically deviate from experimental results, since effects of anharmonicity of the interaction potential are not taken into account and frequency scaling factors of ≈0.9 to 0.95 are typical [54]. For simplicity, we will give only the scaled DFT results in the text. The unscaled calculated DFT values are listed in Table 1 and Table 2. Note that a normal mode of a polyatomic molecule is a linear combination of several internal coordinates, such as bond angle bending and stretching. Since it is quite difficult to fully correctly describe a normal vibration consisting of a number of changing internal coordinates in a concise way, we decided to describe each calculated normal mode via the most pronounced internal coordinate(s) contributing to this vibration. It should be also noted that the experimentally measured IR spectra of the molecules adsorbed in the multilayers are compared to the

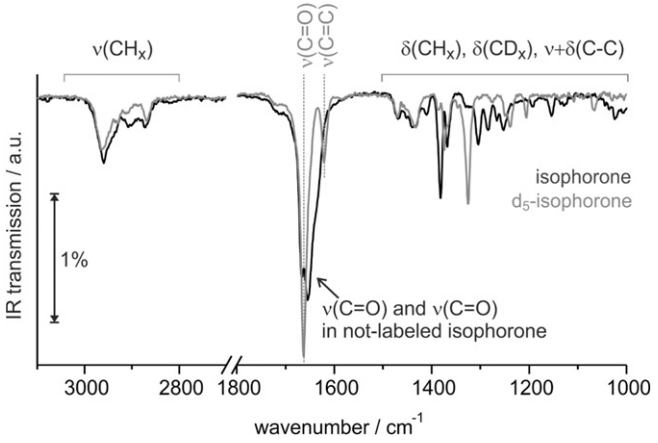

Fig. 2. IR spectra of 3 ML isophorone (black) and d_5-isophorone (gray) at 120 K on Pd(111). The region characteristic for C–H stretching vibrations (3100–2800 cm^{-1}), C = O and C = C stretching vibrations (1800–1600 cm^{-1}), and C–H and C–D deformation and C–C deformation and stretching vibrations (1500–1000 cm^{-1}).

Table 1
Assignment of IR vibration frequencies from DFT calculations and IRAS experiments of normal isophorone and d_5-isophorone in the range of C = O, C = C, and C–H stretching vibrations (3100–1600 cm^{-1}). Vibration modes that strongly change when switching from normal to *d*-labeled isophorone are printed in bold. Vibration modes that are mostly independent from deuterium-labeling are printed with normal intensity.

	Most pronounced internal coordinate(s) of the normal mode	Vibrations isophorone/cm^{-1}			Vibrations d_5-isophorone/cm^{-1}		
		DFT	DFT scaled	IRAS	DFT	DFT scaled	IRAS
	ν(C = O)	1661	1661	1665	1661	1661	1665
	ν(C = C)	**1624**	**1626**	**1655**	**1608**	**1610**	**1620**
A1	ν(CH)	3085	3006		2287	2253	
A2	$\nu_a(CH_3(A))$	3046	2970	2975–2930	3047	2971	2975–2930
A3	$\nu_a(CH_3(C))$	3032	2957		3034	2958	
A4	$\nu_a(CH_3(B))$	3021	2946		3024	2949	
A5	$\nu_a(CH_3(B,C))$	3016	2941		3021	2946	
A6	$\nu_a(CH_3(B,C))$ *+$\nu_a(CH_2(6))$	3011*	2937		3015	2941	
A7	$\nu_a(CH_3(A))$	2990	2917	2910	2990	2917	2910
A8	$2\delta(CH_3)$			2920–2890			2920–2890
A9	**$\nu_a(CH_2(6))$ * + $\nu_a(CH_3(B,C))$**	**3008***	**2934**	**≈2940**	**2229**	**2198**	**2202**
A10	**$\nu_a(CH_2(4))$**	**2955**	**2884**	**≈2885**	**2187**	**2158**	**2184**
A11	$\nu_s(CH_3)$ (B,C) (in phase)	2949	2878	2874–2865	2957	2886	2874–2865
A12	$\nu_s(CH_3)$ (B,C) (out-of-phase)	2945	2874		2948	2877	
A13	$\nu_s(CH_3)$ (A)	2942	2872		2945	2874	
A14	**$\nu_s(CH_2(6))$**	**2928**	**2858**	**≈2820**	**2130**	**2104**	**2087–2079**
A15	**$\nu_s(CH_2(4))$**	**2908**	**2839**		**2124**	**2098**	

ν: stretch, ν_a: asymmetric stretch, ν_s: symmetric stretch.
DFT scaling factor = 0.945.

DFT results obtained for the gas phase. Here, we made an approximation that the differences between the vibrational modes of the unperturbed molecules in the multilayers and in the gas phase are only minor. More accurate calculations should include effects arising from e.g. site symmetry effects, hydrogen-bonding etc., which will be subject of our future investigations.

The stretching modes are labeled with A1 to A15 and the deformation modes with B1 to B20. We will refer to the respective labels in the following discussion, in the tables, as well as in the IR spectra.

3.1.1. C = C and C = O stretching vibrations

The stretching modes of the C = O and the C = C bonds show very pronounced bands in the spectra displayed in Fig. 2. In normal isophorone, the most intense vibration is the C = O stretching mode at 1665 cm^{-1}, which overlaps with the C = C stretching mode at 1655 cm^{-1}. The C = C and C = O stretching bands are clearly separated in the IR spectrum of d_5-isophorone, in which the C = C stretching band appears at 1620 cm^{-1}, exhibiting a shift of 35 cm^{-1} compared to the unsubstituted molecule. The C = O stretching mode appears to be hardly affected by the substitution and remains essentially at the same frequency of 1665 cm^{-1}. The DFT study indicates that the C = O stretching frequency is at 1661 cm^{-1} for both molecules, while the C = C stretching is predicted to shift from 1624 cm^{-1} in normal isophorone to 1608 cm^{-1} in d_5-isophorone. Previously it has been reported that the C = O and C = C stretching vibrations in α,β-unsaturated ketones overlap if the two bonds have *trans* orientation, such as in isophorone. The vibrational frequencies found in gas-phase studies of unlabeled molecules agree well with our results; C = O vibrations have been observed in the range of 1690–1655 cm^{-1} and C = C stretching modes were observed in the 1649–1618 cm^{-1} range [49,50,53]. Furthermore, the lower C = C stretching frequency in d_5-isophorone agrees well with previous studies, which found that the C = C stretching vibration is lowered by 10–20 cm^{-1} for each substituted H atom at the C = C bond [51].

3.1.2. C–H and C–D Stretching Vibrations

Fig. 3 illustrates the experimental IR spectra of normal isophorone and d_5-isophorone in the range of the C–H and C–D stretching vibrations. The C–H and C–D stretching modes show multiple bands and their assignment is more complex due to overlapping bands and weak dynamic dipole moments. A detailed discussion of the C–H and C–C vibrational modes is presented in the SI. Briefly, our DFT study predicts six asymmetric and three symmetric stretching modes for the three CH_3 groups, one asymmetric and one symmetric stretching vibration for each CH_2 or CD_2 groups, and one stretching mode for the CH or CD group. The computed frequencies and the experimentally observed IR vibrations are summarized in Table 1.

The DFT and IRAS results indicate that the stretching vibrations of the CH_3 groups are mostly unaffected by the deuterium-substitution of the ring H atoms. The scaled DFT results show asymmetric stretching vibrations of the CH_3 groups in normal isophorone between 2970 cm^{-1} and 2917 cm^{-1} (from 2971 cm^{-1} to 2817 cm^{-1} in d_5-isophorone) and symmetric stretching vibrations of the same groups in the range from 2878 cm^{-1} to 2972 cm^{-1} (2886–2874 cm^{-1} in d_5-isophorone). Experimentally, broad IR absorption bands are observed from 2975 cm^{-1} to 2930 cm^{-1} and from 2874 cm^{-1} to 2864 cm^{-1} for both molecules.

Vibrational modes of the deuterium-substituted CD_2 groups are found at much lower frequencies than those of the CH_2 groups. The DFT-calculated frequencies of asymmetric CH_2 stretching vibrations are 2934 cm^{-1} and 2884 cm^{-1}, while the same modes of the CD_2 groups are 2198 cm^{-1} and 2158 cm^{-1}. Experimentally, IR absorption bands are found at 2940 cm^{-1} and 2885 cm^{-1} in normal isophorone as well as at 2202 cm^{-1} and 2184 cm^{-1} in d_5-isophorone. The symmetric stretching vibrations of the CH_2 groups are found at 2858 cm^{-1} and 2839 cm^{-1} by DFT, while those of the CD_2 groups appear at 2104 cm^{-1} and 2098 cm^{-1}. By IRAS, vibrations are observed near 2820 cm^{-1} in normal isophorone and at 2087–2079 cm^{-1} in d_5-isophorone.

3.1.3. Region of C–H and C–D deformation vibrations (<1500 cm^{-1})

IR spectra in the range of the deformation vibrations are illustrated in Fig. 4. The vibrational modes are summarized in Table 2. A detailed discussion can be found in the SI.

Asymmetric bending modes of the CH_3 groups B and C are found between 1475 cm^{-1} and 1445 cm^{-1}, while the same modes of group A are observed between 1440 cm^{-1} and 1430 cm^{-1} for both molecules. Symmetric bending vibrations of all three CH_3 groups appear between

Table 2
Assignment of IR vibration frequencies from DFT calculations and IRAS experiments of normal isophorone and d_5-isophorone in the C–H, C–D and C–C deformation and C–C stretching vibrations (1500–1000 cm^{-1}). Vibration frequencies that strongly change when switching from normal to *d*-labeled isophorone are printed in bold. Vibration modes that are mostly independent from deuterium-labeling are printed with normal intensity.

	Most pronounced internal coordinate(s) of the normal mode	Vibrations isophorone/cm^{-1}			Vibrations isophorone-d_5/cm^{-1}		
		DFT	DFT scaled	IRAS	DFT	DFT scaled	IRAS
B1	$\delta_a(CH_3(B,C))$	1458	1469	1475–1445	1457	1468	1475–1445
		1453	1464		1455	1466	
B2	$\delta_a(CH_3(B,C))$	1440*	1452		1432	1445	
	* + $\delta_a(CH_2(4,6))$	1432*	1445		1429	1442	
B3	$\delta_a(CH_3(A))$[1]	1427	1440	1440–1430	1421	1434	1440–1430
		1423	1436		1419	1432	
B4	**$\delta(CH_2(4,6))$ (in-phase) * + $\delta_a(CH_3(B,C))$**	**1409***	**1423**	**1418–1408**	**1044**	**1078**	**1067**
B5	**$\delta(CH_2(4,6))$ (out-of-phase)**	**1397**	**1412**		**1035**	**1069**	
B6	$\delta_s(CH_3(B,C))$ (open-open)	1368	1384	1382	1365	1381	1385 1372
B7	$\delta_s(CH_3(A))$	1355	1372	1368	1351	1368	1368
B8	$\delta_s(CH_3(B,C))$ (open-close)	1347	1364		1344	1361	
B9	ν(C6–C1–C2) ν(C3–C4–C5)				1290	1312	1325(?)
B10	$\Omega(CH_2(4))$ δ(CH) ν(C3–C4)	1334	1352				
B11	$\Omega(CH_2(4,6))$ δ(CH bend) ν(C1–C2)	1297	1317	1304			
B12	$\tau(CH_2(4))$ ν(C6–C1–C2)	1271	1292	1283			
B13	**ν(C–C) in ring**	**1251[a]**	**1274**	**1266**	**1223**	**1247**	**1250**
	[a] + $\Omega(CH_2(4))$	**1234[a,b,c]**	**1257**		**1214**	**1239**	
	[b] + $\Omega(CH_2(6))$			**1253**			**1239**
	[c] + δ(CH)	**1221[c,d,e]**	**1245**		**1200**	**1225**	
	[d] + $\tau(CH_2(4))$						
	[e] + $\tau(CH_2(6))$						
B14	ν(C6–C1–C2) ν(C5–CH_3(C))				1178	1205	1205
B15	ν(C5–CH_3(B)) δ(C–C) $\tau(CH_2(4))$	1170	1197	1192			
B16	$\tau(CH_2(4,6))$	1131	1159	1154			
B17	δ(C–C) all bonds	1113	1143				
B18	$\tau(CH_2(6))$	1101	1131	1133–1123	889	931	
					774	822	
B19	$\tau(CH_2(4))$				832	878	
					821	867	
B20	$\rho(CH_3(A,B,C))$	1016	1051		1024	1059	
		1002	1038		1011	1047	
		988	1025		989	1026	
		972	1010		933	973	
		929	969		920	961	
		920	961		909	950	

ν: stretch, δ: bend, δ_a: asymmetric bend, δ_s: symmetric bend, ω: wag, τ: twist, ρ: rock.
DFT scaling factor = 0.945.
[1] Note that this band strongly shifts in the saturated ketone TMCH in which the immediate environment of CH_3(A) is changed (see Table 4).

1382 cm^{-1} and 1368 cm^{-1}. The bending modes of the CH_2 groups, however, are strongly affected by the deuterium substitution. In normal isophorone, DFT results show CH_2 bending vibrations at 1423 cm^{-1} and 1412 cm^{-1}, while CD_2 bending vibrations are 1078 cm^{-1} and 1069 cm^{-1}. Experimentally, IR absorption bands are observed at 1418–1408 cm^{-1} for normal isophorone and near 1067 cm^{-1} for d_5-isophorone.

3.2. Isophorone at sub-monolayer coverage

3.2.1. Isophorone on pristine Pd(111)

Fig. 5 displays IR spectra of d_5-isophorone adsorbed on Pd(111) at 120 K at coverages ranging from the multilayer to the sub-monolayer regime. While the IR spectra of isophorone at multilayer coverages are dominated by molecules in isophorone ice, the sub-monolayer spectra show the vibrations of isophorone molecules directly interacting with the Pd surface. The adsorption geometry of molecules on metal surfaces can be deduced from their IR spectra based on the metal surface selection rule (MSSR) [24,26]. According to the MSSR, only the component of a dynamic dipole moment perpendicular to the metal surface can be detected, while vibrations parallel to the surface are strongly attenuated by an image dipole in the metal substrate. Changes in the intensity distribution between C = C, C = O and C–H vibrations with decreasing isophorone coverage indicate the transition from a more random orientation in multilayers to a favored geometry of molecules attached to Pd(111).

At the lowest coverage of d_5-isophorone on Pd(111) (1/6 ML), there are significant absorption bands dectected in the C–H stretching and

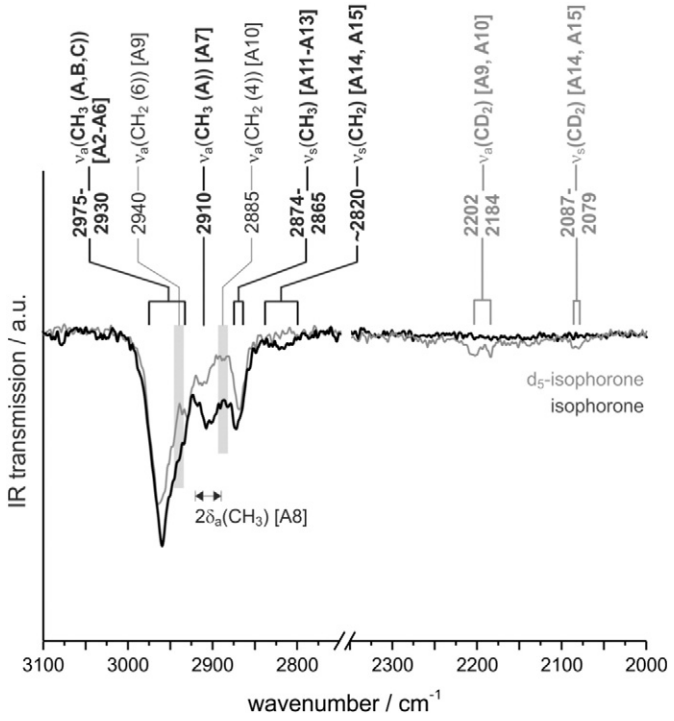

Fig. 3. IR spectra of 3 ML of normal and d_5-isophorone adsorbed at 120 K on Pd(111) from 3100 to 2750 cm^{-1} (C–H stretching) and 2400–2000 cm^{-1} (C–D stretching). Clearly assigned vibrations are indicated with bold printed labels, more tentative assignments are labeled with normal thickness.

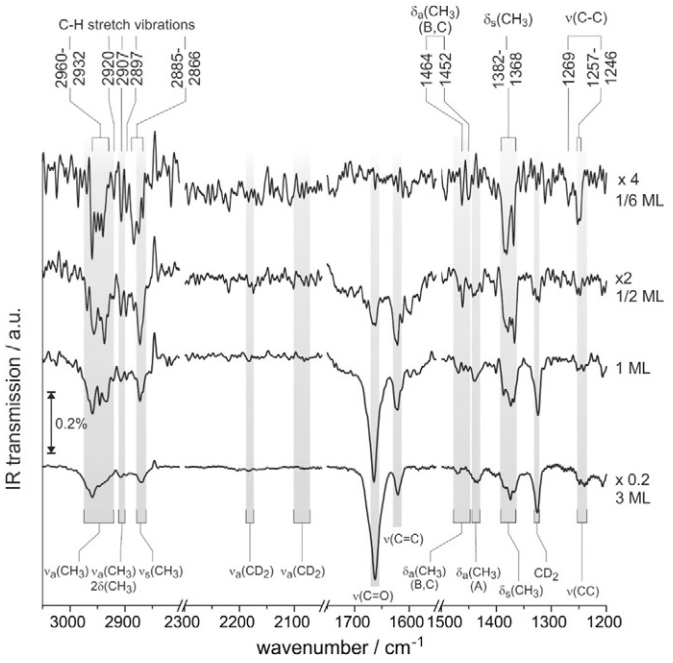

Fig. 5. IR spectra d_5-isophorone adsorbed at 120 K on Pd(111) from 3050 to 2800 cm^{-1} (C–H stretching), 2300–2050 cm^{-1} (C–D stretching), 1800–1600 cm^{-1} (C = C and C = O stretching), and 1500–1000 cm^{-1} (C–H, C–D, C–C deformation and C–C stretching) at different coverages. Vibrations in isophorone ice are indicated close to 3 ML spectrum (lowest trace). The wavenumbers of the IR vibrations at the lowest coverage (1/6 ML) (topmost trace) are given on top.

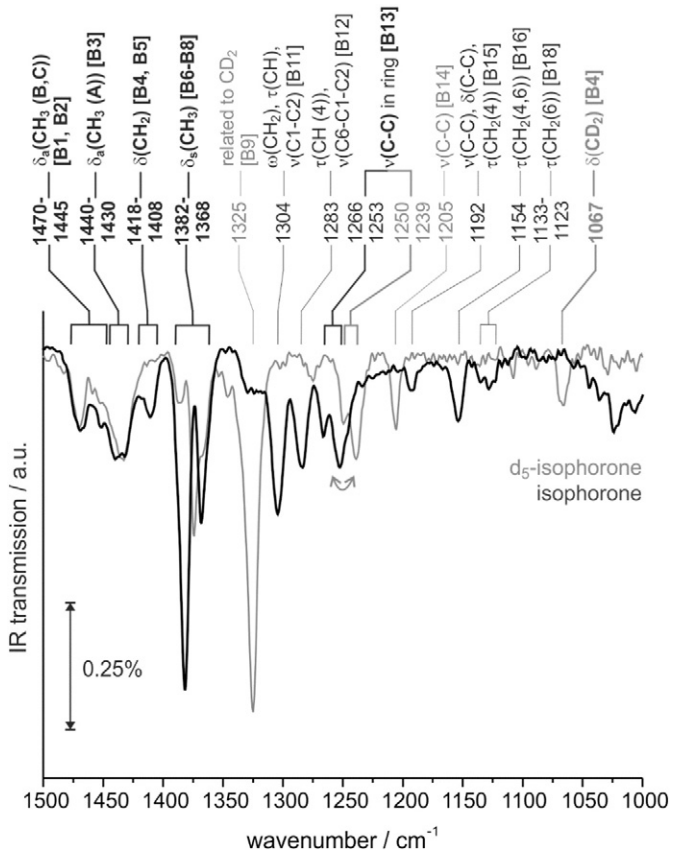

Fig. 4. IR spectra of 3 ML of normal and d_5-isophorone adsorbed at 120 K on Pd(111) from 1500 to 1000 cm^{-1} Clearly assigned vibrations are indicated with bold printed labels, more tentative assignments are labeled with normal thickness.

deformation regions; however, there are no band detected for the C = O or C = C stretching modes. This intensity distribution is in sharp contrast to the observation at multilayer coverage, where the most intense vibration is the C = O stretching mode. The absence of IR absorption in the C = O and C = C stretching region indicates that these bonds are either orientated parallel to the metal surface and cannot be seen in IRAS because of the MSSR or are strongly perturbed by the interaction with the Pd(111) surface. The orientation of the unsaturated C = C and C = O bonds has been studied in more detail by previous NEXAFS and IRAS experiments [22]. NEXAFS experiments confirmed that the C = C and C = O bonds stay intact, but are oriented parallel to the Pd(111) surface plane at a coverage of 0.2 ML. With increasing coverage, the intensities of the IR bands assigned to the C = O and C = C stretching vibrations strongly increase. For a coverage of 1/2 ML, the C = C stretching peak at 1620 cm^{-1} is more pronounced than the C = O stretching band around 1665 cm^{-1}. With further increasing coverage, the C = O stretching band increases rapidly and becomes the most intense peak at full monolayer coverage and above. The ratio of the C = O to C = C stretching vibration at multilayer coverage is ~6–8. The strong C = C stretching band and the low intensity of the C = O stretching band at 1/2 ML point to a strongly tilted C = C bond, while the orientation of C = O bond remains nearly parallel to the surface — this observation is in excellent agreement with our earlier NEXAFS study.

At sub-monolayer coverage, pronounced IR absorption is observed at 2960–2932 cm^{-1} and at 2885–2866 cm^{-1} and thus in the range of the CH_3 (and CH_2) asymmetric and symmetric stretching modes. IR absorption was not been observed at 2885–2874 cm^{-1} in multilayer isophorone. Further IR absorption features can be recognized at 2920 cm^{-1}, 2907 cm^{-1}, and 2897 cm^{-1}. The absorption band at 2907 cm^{-1} is most likely related to an overtone of a CH_3 asymmetric bending mode and will be discussed further in Section 3.2.2. Among the CH_3 bending modes, symmetric modes are intense at 1382–1368 cm^{-1}, while the asymmetric modes are hardly detectable at

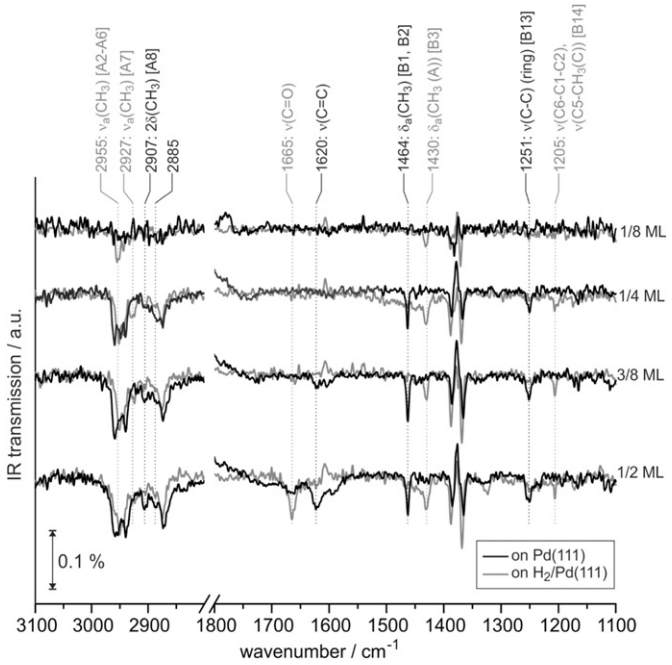

Fig. 6. IR spectra d_5-isophorone adsorbed at 120 K on Pd(111) (black traces) and on hydrogen pre-covered Pd(111) (gray traces) in the frequency range 3100–2800 cm^{-1} (C–H stretching) and 1800–1600 cm^{-1} (C = C and C = O stretching), 1500–1100 cm^{-1} (C–H, C–D, C–C deformation and C–C stretching at sub-monolayer coverages. Vibrations that are more pronounced in isophorone on pristine Pd(111) are indicated with black labels, vibrations that are more pronounced on hydrogen pre-covered Pd(111) are indicated with gray labels.

1464 cm^{-1} and 1452 cm^{-1}. This intensity distribution between vibrations of the same functional group points to a strongly favored adsorption geometry, with some CH_3 dynamic dipole moments parallel to the metal surface and others strongly inclined with respect to the surface plane. In fact, a strong dynamic dipole perpendicular to the surface for the symmetric bending mode and parallel dipole moment for the asymmetric bending mode points to a CH_3 group which is facing away from the surface and is strongly inclined with respect to the C = C–C = O plane of isophorone. IR absorption bands near 2885–2874 cm^{-1}, which are unique for low coverage, could either point to a shifted CH_3 symmetric stretching frequency and thus to a perturbation of a CH_3 group; or to a CH_2 asymmetric stretching mode and thus to dehydrogenation of a CH_3 group. Note that intact d_5-isophorone molecules do not have unlabeled CH_2 groups.

3.2.2. Isophorone on hydrogen pre-covered Pd(111)

In order to study the effect of co-adsorbed hydrogen on the interaction of isophorone with Pd(111), the Pd(111) surface was pre-exposed to 100 L H_2 at 120 K. Previously it has been shown that H_2 rapidly dissociates on the Pd(111) surface, forming a 1 × 1 overlayer of H atoms adsorbed on threefold-hollow sites (formal surface coverage: 1 H atom per 1 Pd surface atom) [55–57]. Note that no subsurface hydrogen species can be formed under these conditions. Fig. 6 shows IR spectra of d_5-isophorone adsorbed on pristine Pd(111) (black traces) and on hydrogen-saturated Pd(111) (red traces) at 120 K, with d_5-isophorone coverages ranging from 1/8 ML to 1/2 ML. While the spectra of d_5-isophorone multilayers on pristine and hydrogen pre-covered Pd(111) are similar, significant differences are observed at sub-monolayer coverages. Black labels indicate IR absorption bands that are more pronounced on the clean Pd(111) surface, gray labels mark peaks having higher intensity on hydrogen pre-covered Pd(111) in the low coverage limit.

At the lowest coverages, clearly different C–H vibrational modes appear on pristine and hydrogen pre-covered Pd(111). Stronger IR absorption of isophorone on hydrogen pre-covered Pd(111) is observed at 2955 cm^{-1} and 2927 cm^{-1} (CH_3 asymmetric stretching modes) and at 1430 cm^{-1} (the CH_3 asymmetric bending mode of group A). In contrast, on pristine Pd(111), peaks appear in the C–H stretching region at 2907 cm^{-1} and 2885 cm^{-1}. The vibrational band at 2907 cm^{-1} is most likely related to the overtone of the CH_3 asymmetric bending mode at 1464 cm^{-1}, which is also unique for molecules on pristine Pd(111). Moreover, the C–C stretching modes near 1251 cm^{-1} are more pronounced on the clean surface, while the mode at 1205 cm^{-1} is more intense on the hydrogen pre-covered surface.

According to the MSSR we conclude that the different distribution of IR absorption intensities on pristine and H_2 pre-covered Pd(111) point to different adsorption geometries of isophorone on both surfaces. Especially the differences in the C–H stretching modes indicate significant changes in the orientation of the CH_3 groups with respect to the surface in the presence of hydrogen. Furthermore, not only geometric effects, but also perturbation and/or chemical transformation of isophorone could yield different spectroscopic signatures on each surface. The IR absorption near 2885 cm^{-1}, which is unique for isophorone on pristine Pd(111) at low coverage, might point to conversion of a CH_3 to a CH_2 group. This pathway seems to be suppressed in the presence of H_2.

Note that the relative intensities of the C–H vibrational bands might slightly differ for different measurements at nominally the same surface coverage, which might be due to the strong dipole coupling effects and/or variation of the surface coverage.

3.3. IR vibrations and adsorption of TMCH

The product of C = C bond hydrogenation in isophorone is the saturated ketone 3,3,5-trimethylcyclohexanone(TMCH). In this section, we assign the IR vibrational modes of TMCH adsorbed on Pd(111) for comparison to isophorone.

3.3.1. Assignment of vibrations in TMCH multilayers

As discussed above, scaling the DFT-calculated IR spectra is necessary to fit the calculated values to the experimentally observed IR vibrations. In the following discussion, DFT results are scaled by the factor 0.954 around 1630 cm^{-1}. The unscaled values can be found in Table 3 and Table 4. Stretching modes of TMCH are labeled with C1 to C15 and deformation modes with D1 to D28. We refer to the respective labels in the following discussion, in the tables, as well as in the IR spectra. A comparison of the IR spectra of TMCH and isophorone multilayers is shown in Fig. 7. Most importantly, there are two different peaks in the C = O stretching region that likely result from different TMCH species. We assign the strong peak at 1713 cm^{-1} to C = O stretching in TMCH ice since it grows continuously with increasing exposure, and the band at 1648 cm^{-1} to a C = O stretching mode from sub-monolayer TMCH. These peaks will be discussed in more detail in the following section.

The vibrational modes of TMCH are summarized in Table 3. The IR spectrum of multilayer TMCH on Pd(111) is plotted together with the IR spectrum of the same coverage of isophorone in Fig. 7. Fig. 7 also shows the assignment of selected vibrational modes. For a detailed discussion of the vibrational modes of TMCH we refer to the SI.

3.3.2. TMCH at sub-monolayer coverage

Fig. 8 shows IR spectra of TMCH on Pd(111) at 120 K from 1800 cm^{-1} to 1200 cm^{-1} at different coverages. The coverage-dependent evolution of IR absorption features gives detailed insights into the binding and the geometry of TMCH on Pd(111). According to the MSSR, only the projection of the dynamic dipole moment perpendicular to the surface can be measured by IRAS.

The IR absorption intensities in the C–H stretching (not shown here) and the C–H deformation regions grow roughly monotonically with

Table 3
Assignment of IR vibrations of TMCH from DFT and IRAS studies in the range of the C = C, C = O, and C–H stretching vibrations (3100–1600 cm^{-1}).

	Most pronounced internal coordinate(s) of the normal mode	Vibrations TMCH/cm^{-1}		
		DFT	DFT scaled	IRAS
	ν(C = O)	1693	1690	1713
	ν(C = O)			1648
C1	ν_a(CH_3(B))	3026	2962	2975–2940
C2	ν_a(CH_3(A))	3023	2959	
C3	ν_a(CH_3(B))	3021	2957	
	ν_a(CH_3(C)			
	ν_a(CH_2(6))			
C4	ν_a(CH_2(2))	3018	2954	
	ν_a(CH_3(A,C))			
	ν(CH(3))			
C5	ν_a(CH_3(B)	3016	2952	
	ν_a(CH_3(C))			
	ν_a(CH_2(2,6))			
C6	ν_a(CH_3(C)	3013	2949	
	ν_a(CH_3(B))			
	ν_a(CH_2(6))			
C7	ν_a(CH_3(A))	3012	2948	
	ν_a(CH_2(6))			
	ν_a(CH_3(C)			
	ν_a(CH(3))			
	ν_a(CH_2(2)			
C8	ν_a(CH_2(4))	2967	2905	2913
	ν(CH(3))			
C9	ν_s(CH_3(B)	2953	2892	2880–2865
C10	ν_s(CH_3(A)	2946	2885	
	ν(CH(3))			
C11	ν_s(CH_3(C)	2943	2883	
C12	ν(CH(3))	2936	2876	
	ν_s(CH_2(2,4,6))			
C13	ν_s(CH_2(6))	2931	2871	
C14	ν_s(CH_2(2))	2916	2857	
	ν_s(CH_2(4))			
	ν(CH(3))			
C15	ν_s(CH_2(4))	2912	2853	≈ 2840
	ν_s(CH(3))			
	ν_s(CH_2(2))			

ν: stretch, ν_a: asymmetric stretch, ν_s: symmetric stretch.
DFT scaling factor = 0.954.

increasing TMCH exposure. In the C = O stretching region, however, there are non-trivial changes in the bands observed with increasing TMCH exposure. At the lowest TMCH exposure (1/12 ML), a sharp band at 1648 cm^{-1} is detected and a smaller, broad band is observed at 1747 cm^{-1}. The band at 1648 cm^{-1} grows slightly with increasing exposure and is saturated at 1/6 ML exposure. The band at 1747 cm^{-1} does not change intensity up to 1/3 ML, and then disappears at coverages greater than 1/3 ML. A small band at 1701 cm^{-1} appears at 1/6 ML exposure and increases slightly in intensity up to 1/3 ML, but does not appear to grow further with increasing exposure. At 1/2 ML exposure, a bands at 1713 cm^{-1} appears and continues to grow with increasing exposure.

The IRAS series shown in Fig. 8 gives valuable information about the interaction of TMCH with the Pd(111) substrate. First, there are several different peaks in the C = O stretching region that likely result from different TMCH species. We can assign the strong band at 1713 cm^{-1}, which grows continuously with increasing exposure beyond 1/2 ML, to C = O stretching in TMCH ice. We assign the band at 1648 cm^{-1}, which is observed at the lowest exposure (1/12 ML) and is saturated by 1/6 ML, to a C = O stretching mode from sub-monolayer TMCH. The C = O stretching modes at 1701 cm^{-1} and 1747 cm^{-1} are most likely related to TMCH species in the intermediate coverage range between sub-monolayer and multilayer ice, probably the second layer. Finally, the strong intensity of the C = O vibration at 1648 cm^{-1} even at the lowest TMCH exposure (1/12 ML) indicates that the C = O bond in TMCH is strongly tilted with respect to the Pd(111) surface plane at sub-monolayer coverage. These results indicate that at low coverage TMCH adsorbs close to perpendicularly to Pd(111) plane through the C = O group, strongly perturbing the C = O stretching vibration. With increasing TMCH coverage, several more TMCH species are formed, giving rise to new C = O vibrational bands. Second, the bands in the C–H stretching and the C–H deformation regions grow roughly monotonically with increasing TMCH exposure, and there is no indication that these vibrational modes are strongly affected by the Pd(111) substrate.

Below 1500 cm^{-1}, all IR absorption features of TMCH become weaker with decreasing coverage. In contrast to isophorone, a selective disappearance of only some vibrations modes is not observed; the decrease in intensity is evenly distributed through all IR absorption features.

To better understand the influence of the Pd(111) substrate on the C = O stretching modes of TMCH, we have performed DFT calculations of the IR spectra of TMCH in the gas phase and of an isolated TMCH molecule adsorbed on Pd(111), which are shown in Fig. 9. The position of the calculated C = O stretching mode of gas-phase TMCH (1694 cm^{-1}) is 83 cm^{-1} higher in wavenumber than that of TMCH adsorbed on Pd(111) (1611 cm^{-1}), indicating a strong perturbation of the C = O vibrational mode of TMCH by interaction with the Pd(111) surface. Also shown in Fig. 9 are the IR spectra of gas-phase TMCH from the NIST Chemistry WebBook [58] and TMCH (1.5 ML exposure at 120 K) adsorbed on Pd(111). The position of the calculated C = O vibrational band in gas-phase TMCH (1694 cm^{-1}) is not the same as that of gas-phase TMCH from the NIST database (1730 cm^{-1}). Also, the

Table 4
Assignment of IR vibration modes of TMCH in the range from 1500 cm^{-1} to 1000 cm^{-1}.

	Most pronounced internal coordinate(s) of the normal mode	Vibrations TMCH/cm^{-1}		
		DFT	DFT scaled	IRAS
D1	$\delta_a(CH_3(B,C))$	1457	1465	1475–1445
	$\delta_a(CH_3(A))$	1452	1459	
D2	$\delta_a(CH_3(A))$	1446	1455	
	$\delta_a(CH_3(B,C))$	1445	1454	
D3	$\delta_a(CH_3(B,C))$	1441	1450	
	$\delta_a(CH_3(A))$	1433	1442	
	$\delta(CH_2(4,6))$			
D4	$\delta(CH_2(4))$	1426	1435	1435–1410
	$\delta(CH_2(2,6))$			
	$\delta_a(CH_3(B,C))$			
D5	$\delta(CH_2(2,6))$ (in-phase)	1410	1420	
	$\delta(CH_2(4))$ (out-of-phase)			
D6	$\delta(CH_2(2,6))$ (out-of-phase)	1403	1413	
D7	$\delta_s(CH_3(B,C))$ (open-open)	1369	1381	1388
				1376
D8	$\delta_s(CH_3(A))$	1359	1371	1364
D9	$\delta_s(CH_3(B,C))$ (open-close)	1348	1361	
D10	$\delta(CH(3))$	1333	1347	1336
	$\omega(CH_2(2,4))$			
D11	$\delta(CH(3))$	1314	1329	1316
	$\tau(CH_2(2,4))$			
D12	$\nu(C5\text{-}CH_3(C))$	1289	1305	1300
	$\omega(CH_2(4,6))$			
	$\delta(CH(3))$			
D13	$\nu(C5\text{-}CH_3(B))$	1274	1290	
	$\tau(CH_2(2,4,6))$			
	$\delta(CH(3))$			
D14	$\nu_s(C6–C1–C2)$	1259	1276	1282–1254
	$\omega(CH_2(2,4,6))$			
	$\delta(CH(3))$			
D15	$\nu_a(C6–C1–C2)$	1242	1260	
	$\omega(CH_2(2,4,6))$			
D16	$\nu(C–C) + \delta(C–C)$	1233	1251	
	$\tau(CH_2(2,4,6))$			
D17	$\nu(C–C)$ in ring	1207	1226	1235–1222
	$\tau(CH_2(2,4,6))$			
D18	$\nu(C4–C5–C6)$	1197	1217	
	$\omega(CH_2(2,4,6))$			
D19	$\nu(C5–CH_3(B))$	1154	1177	
	$\rho(CH_3(A,B,C))$			
	$\omega(CH_2(6))$			
D20	$\nu(C3–C4)$	1134	1157	1150–1130
	$\tau(CH_2(2,4,6))$			
	$\rho(CH_3(A,B,C)$			
D21	$\nu(C2–C3–C4)$	1117	1141	
	$\rho(CH_3(A)$			
D22	$\nu(C5–C6–C1–C2)$	1061	1087	1095–1078
	$\tau(CH_2(2,4,6))$			
	$\rho(CH_3(A,C))$			
D23	$\nu(C3–CH_3(A))$	1050	1077	
	$\rho(CH_3(A,B,C))$			
D24	$\rho(CH_3(A,C))$	1018	1046	
	$\delta(C–C) + \nu(C–C)$			
	$\tau(CH_2(2,6))$			
D25	$\rho(CH_3(B,C))$	988	1018	
D26	$\rho(CH_3(A))$	962	993	
	$\rho(CH_3(B,C))$	943	975	
D27	$\rho(CH_3(B,C))$	917	950	
	$\rho(CH_3(A))$	909	942	
D28	$\rho(CH_3(A,B,C))$	887	921	
	$\nu(C3–C4)$			

ν: stretch, δ: bend, δ_a: asymmetric bend, δ_s: symmetric bend, ω: wag, τ: twist, ρ: rock.
DFT scaling factor = 0.954.

position of the calculated C = O stretching mode for an isolated TMCH molecule adsorbed on Pd(111) (1611 cm^{-1}) is not the same as the C = O stretching mode from sub-monolayer TMCH on Pd(111) that we measured (1648 cm^{-1}). However, the difference in the position of the calculated C = O stretching mode in gas-phase TMCH to the calculated C = O stretching mode of an isolated TMCH molecule on Pd(111) (83 cm^{-1}) is almost exactly the same as the difference in the position of the C = O stretching mode in gas-phase TMCH from the NIST database and sub-monolayer TMCH on Pd(111) from this work (82 cm^{-1}).

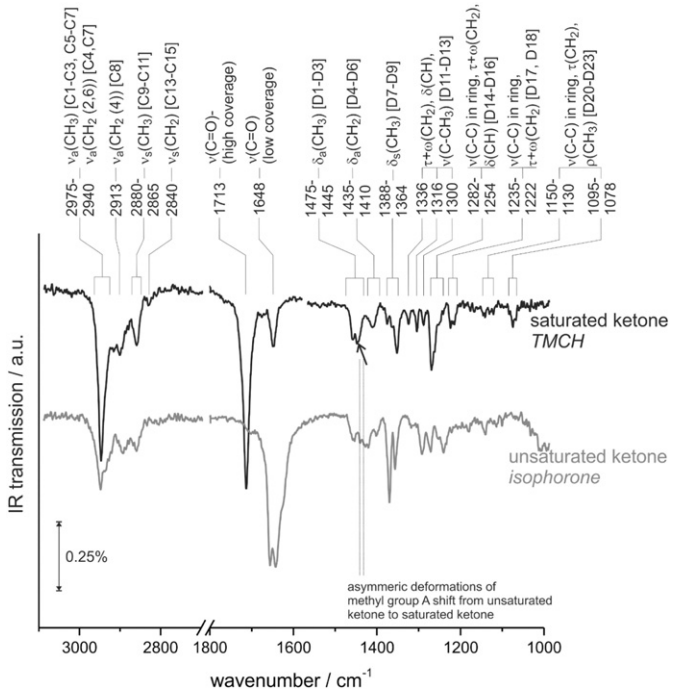

Fig. 7. IR spectra of 1.5 ML of TMCH (black) and isophorone (gray) adsorbed at 120 K on Pd(111) in the frequency range 3100–2700 cm^{-1} (C–H stretching), 1800–1600 cm^{-1} (C = C and C = O stretching), and 1500–1000 cm^{-1} (C–H and C–C deformation and C–C stretching).

Combining the experimental IRAS results and DFT calculations, a clearer picture of the interaction between TMCH and Pd(111) emerges, which is very different from that of isophorone. The C–H stretching and C–H deformation regions grow roughly monotonically with increasing coverage, pointing to a possibly less strict ordering of molecules on the surface. TMCH interacts with the Pd(111) surface primarily through the C = O group. At low coverage, TMCH adsorbs roughly perpendicular to Pd(111) through the strongly perturbed C = O group, giving rise to a C = O vibrational band that is strongly shifted by ≈82 cm^{-1} to lower wavenumber relative to that of gas-phase TMCH. At intermediate coverage between sub-monolayer and multilayer ice, two new C = O vibrational bands appear at 1747 cm^{-1} and 1701 cm^{-1}. The origin of these peaks is not fully clear, however, they may arise from the second layer of TMCH molecules. A C = O vibrational band from multilayer TMCH ice appears at 1713 cm^{-1}, which is 17 cm^{-1} lower in wavenumber than the C = O stretching mode of gas-phase TMCH, and continues to grow with further increasing coverage.

4. Conclusions

The adsorption of the unsaturated ketone isophorone and its hydrogenation product, the saturated ketone TMCH, on Pd(111) were investigated in this work. IR vibration modes of isophorone, deuterium-labeled (d_5-) isophorone and TMCH were studied in the range from 3000 cm^{-1} to 1000 cm^{-1} by IRAS and DFT studies. Detailed assignment of IR vibrations was achieved for the first time for normal and d_5-isophorone as well as TMCH at multilayers coverages.

Investigation of normal and d_5-isophorone allowed for better assignment of vibrational bands:

- C = C and C = O stretching modes are well-separated in d_5-isophorone, but are strongly overlapping in normal isophorone,
- CH_2 stretching and bending modes can be distinguished from CH_3 stretching and bending vibrations, and

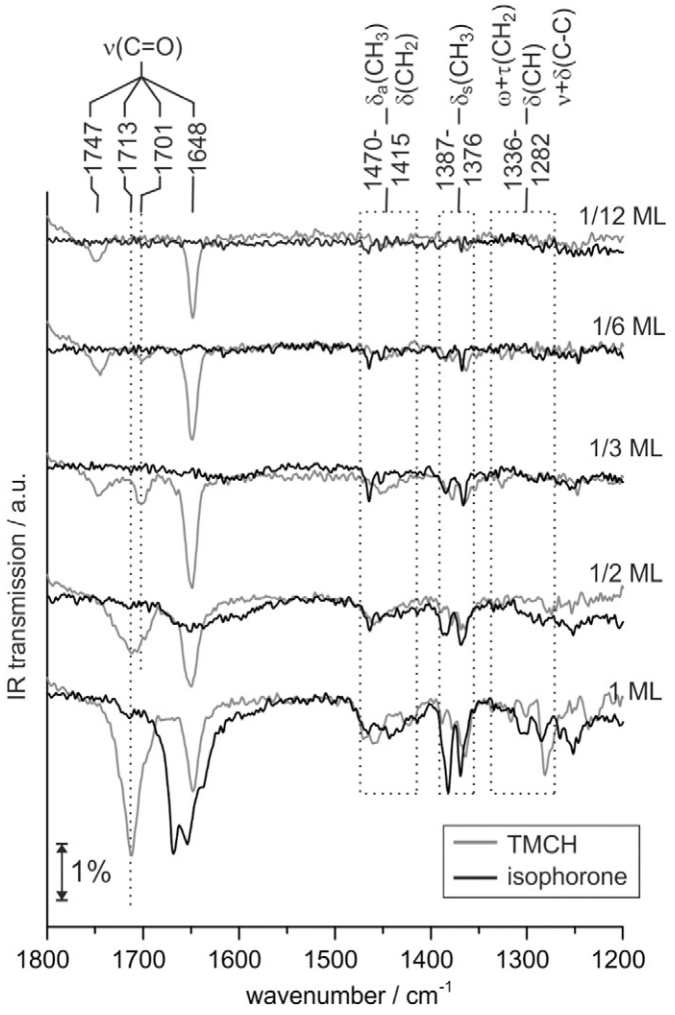

Fig. 8. IR spectra of TMCH and d_5-isophorone adsorbed at 120 K on Pd(111) at 1800–1600 cm^{-1} (C = C and C = O stretching) and 1500–1000 cm^{-1} (C–H, C–D, C–C deformation and C–C stretching) at coverages from 1/12 ML (topmost trace) to 1 ML (lowest trace).

- C–C stretching vibrations are separated from CH_2 wag, CH_2 twist, and CH bend modes.

Vibration frequencies of isolated isophorone and TMCH molecules from DFT + vdW calculations agree well with the experimentally observed IR absorption features at multilayer coverages. A detailed assignment of vibrational modes between 3000 cm^{-1} and 1000 cm^{-1} was presented for the three molecules.

The coverage dependent evolution of IR vibrational bands provides deep insights into the structure of isophorone on Pd(111):

- At the lowest isophorone coverage, we observed a flat-lying adsorption geometry with the C = C and C = O bonds being oriented parallel to the surface plane and at least one CH_3 group facing away from the Pd. This observation suggests that isophorone preserves the in-plane configuration of the conjugated π-system in the low coverage limit. However, dehydrogenation of a CH_3 group to CH_2 appears to be possible.
- For intermediate sub-monolayer coverages, the in-plane structure of the isophorone ring adsorbed on pristine Pd(111) was observed to be strongly distorted. The C = C bond becomes noticeably tilted with respect to the surface plane, while the C = O bond remains still oriented flat on the surface.

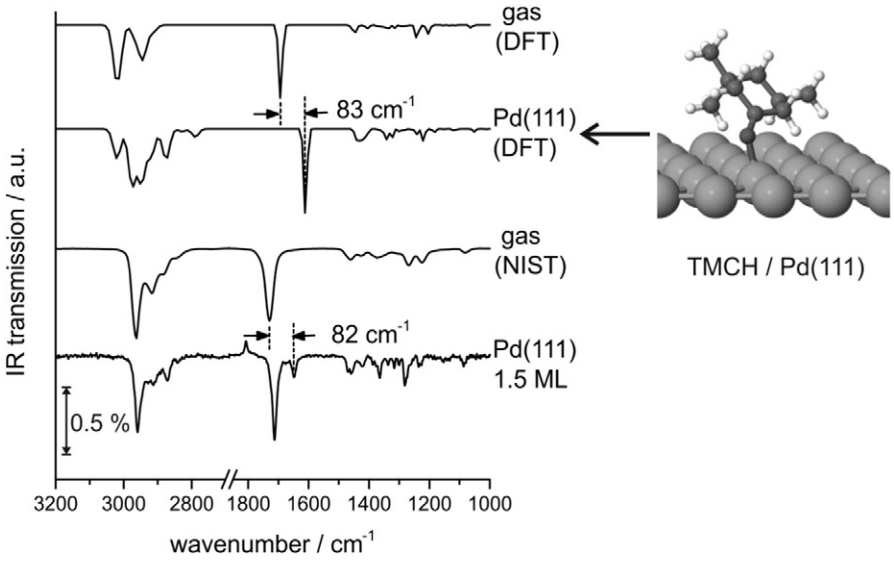

Fig. 9. Comparison of C = O stretching vibration in TMCH in different states (from top down): calculated by DFT in gas phase and adsorbed on Pd(111), gas phase spectrum according to NIST [58], and IRAS measurement on multilayer coverage of TMCH on Pd(111) at 120 K.

The IR spectra indicate that the adsorption of isophorone is significantly affected by the presence of pre-adsorbed hydrogen:

- At intermediate isophorone coverages, the molecular structure is similar to that of gas-phase isophorone.
- At low coverages of isophorone, the intensity ratio of the C–H vibrations strongly points to different orientation of the $–CH_3$ groups as compared to pristine Pd(111). The molecules appear to be more perturbed on the clean Pd(111) surface than on the hydrogen-precovered surface.
- The hydrogen-induced changes in the orientation of unsaturated bonds may have important implications for selective hydrogenation of either the C = C or the C = O bond, i.e. via changing the typical distances of the C = C vs. C = O bonds to the surface and thus effecting the degree of their perturbation and the hydrogenation probability.

We found pronounced differences in the structures of the saturated ketone TMCH and the unsaturated ketone isophorone adsorbed on Pd(111):

- TMCH adsorbs in a strongly tilted geometry with respect to the Pd(111) surface plane, interacting with the surface primarily through the C = O group.
- At the lowest TMCH coverage, the species give rise to a C = O vibrational band that points to a considerably weakened C = O bond.
- At intermediate TMCH coverage, species with less perturbed C = O bonds also appear.
- The C–H vibrational bands grow roughly monotonically with increasing coverage, which might point to less perturbed C–H bonds and a less strict ordering of molecules on the surface.
- The strong changes in the adsorbate's structure going from the unsaturated to the saturated ketone (isophorone to TMCH) may play a crucial role in the selectivity of C = C vs. C = O bond hydrogenation in α,β-unsaturated carbonyl compounds.

Acknowledgments

S.S. acknowledges support from the Fonds der Chemischen Industrie for the Chemiedozentenstipendium and the European Research Council (ERC Starting Grant 335205 ENREMOS). A.T. acknowledges support from the European Research Council (ERC Starting Grant VDW-CMAT).

References

[1] M.T. Pirnot, D.A. Rankic, D.B.C. Martin, D.W.C. MacMillan, Science 339 (2013) 1593.
[2] Y. Zhu, H.F. Qian, B.A. Drake, R.C. Jin, Angew. Chem. Int. Ed. 49 (2010) 1295.
[3] S. Fleischer, S.L. Zhou, K. Junge, M. Beller, Angew. Chem. Int. Ed. 52 (2013) 5120.
[4] M.G. Hitzler, F.R. Smail, S.K. Ross, M. Poliakoff, Org. Process. Res. Dev. 2 (1998) 137.
[5] T. Sato, C.V. Rode, O. Sato, M. Shirai, Appl. Catal. B Environ. 49 (2004) 181.
[6] D.I. Enache, G.J. Hutchings, S.H. Taylor, E.H. Stitt, Catal. Today 105 (2005) 569.
[7] A. Tungler, K. Fodor, T. Mathe, R.A. Sheldon, in: H.U. Blaser, A. Baiker, R. Prins (Eds.), Heterogeneous Catalysis and Fine Chemicals Iv, 108, Elsevier Science Bv, Amsterdam 1997, p. 157.
[8] M. Studer, H.U. Blaser, C. Exner, Adv. Synth. Catal. 345 (2003) 45.
[9] H.U. Blaser, B. Pugin, F. Spindler, J. Mol. Catal. A Chem. 231 (2005) 1.
[10] T. Mallat, E. Orglmeister, A. Baiker, Chem. Rev. 107 (2007) 4863.
[11] A. Tungler, G. Fogassy, J. Mol. Catal. A Chem. 173 (2001) 231.
[12] T. Tarnai, A. Tungler, T. Mathe, J. Petro, R.A. Sheldon, G. Toth, J. Mol. Catal. A Chem. 102 (1995) 41.
[13] G. Farkas, K. Fodor, A. Tungler, T. Mathe, G. Toth, R.A. Sheldon, J. Mol. Catal. A Chem. 138 (1999) 123.
[14] A. Tungler, Y. Nitta, K. Fodor, G. Farkas, T. Mathe, J. Mol. Catal. A Chem. 149 (1999) 135.
[15] E. Sipos, A. Tungler, React. Kinet. Catal. Lett. 80 (2003) 365.
[16] E. Sipos, A. Tungler, G. Fogassy, J. Mol. Catal. A Chem. 216 (2004) 171.
[17] M. Fodor, A. Tungler, L. Vida, React. Kinet. Catal. Lett. 90 (2007) 413.
[18] S. Li, E.S. Zhan, Y. Li, Y.D. Xu, W. Shen, J. Catal. Today 131 (2008) 347.
[19] S.K. Beaumont, G. Kyriakou, D.J. Watson, O.P.H. Vaughan, A.C. Papageorgiou, R.M. Lambert, J. Phys. Chem. C 114 (2010) 15075.
[20] D.J. Watson, R. Jesudason, S.K. Beaumont, G. Kyriakou, J.W. Burton, R.M. Lambert, J. Am. Chem. Soc. 131 (2009) 14584.
[21] W. Liu, A. Savara, X. Ren, W. Ludwig, K.-H. Dostert, S. Schauermann, A. Tkatchenko, H.-J. Freund, M. Scheffler, J. Phys. Chem. Lett. 3 (2012) 582.
[22] K.-H. Dostert, C.P. O'Brien, W. Riedel, A. Savara, W. Liu, M. Oehzelt, A. Tkatchenko, S. Schauermann, J. Phys. Chem. C 118 (2014) 27833.
[23] V.G. Ruiz, W. Liu, E. Zojer, M. Scheffler, A. Tkatchenko, Phys. Rev. Lett. (2012) 108.
[24] F.M. Hoffmann, Surf. Sci. Rep. 3 (1983) 107.
[25] S.A. Francis, A.H. Ellison, J. Opt. Soc. Am. 49 (1959) 131.
[26] P. Hollins, J. Pritchard, Prog. Surf. Sci. 19 (1985) 275.
[27] J.M. Libuda, J. Hartmann, H.J. Freund, Rev. Sci. Instrum. 71 (2000) 4395.
[28] V.G. Ruiz, W. Liu, E. Zojer, M. Scheffler, A. Tkatchenko, Phys. Rev. Lett. 108 (2012) 146103.
[29] V. Blum, R. Gehrke, F. Hanke, P. Havu, V. Havu, X. Ren, K. Reuter, M. Scheffler, Comput. Phys. Commun. 180 (2009) 2175.
[30] W. Liu, A. Tkatchenko, M. Scheffler, Acc. Chem. Res. 47 (2014) 3369.
[31] W. Liu, S.N. Filimonov, J. Carrasco, A. Tkatchenko, Nat. Commun. (2013) 4.
[32] W. Liu, J. Carrasco, B. Santra, A. Michaelides, M. Scheffler, A. Tkatchenko, Phys. Rev. B (2012) 86.
[33] E. van Lenthe, E.J. Baerends, J.G. Snijders, J. Chem. Phys. 101 (1994) 9783.
[35] J.J. Fox, A.E. Martin, Proc. R. Soc. Lond. A Math. Phys. Sci. 175 (1940) 0208.
[36] J.J. Fox, A.E. Martin, Proc. R. Soc. Lond. A Math. Phys. Sci. 167 (1938) 0257.

[37] N. Sheppard, D.M. Simpson, Q. Rev. Chem. Soc. 7 (1953) 19.
[38] R.A. Macphail, H.L. Strauss, R.G. Snyder, C.A. Elliger, J. Phys. Chem. 88 (1984) 334.
[39] J.H. Schachtschneider, R.G. Snyder, Spectrochim. Acta 19 (1963) 117.
[40] R.G. Snyder, J.H. Schachtschneider, Spectrochim. Acta 19 (1963) 85.
[41] N.B. Colthup, Appl. Spectrosc. 34 (1980) 1.
[42] R.G. Snyder, M.C. Goh, V.J.P. Srivatsavoy, H.L. Strauss, D.L. Dorset, J. Phys. Chem. 96 (1992) 10008.
[43] M. Shimomura, K. Song, J.F. Rabolt, Langmuir 8 (1992) 887.
[44] H.L. McMurry, V. Thornton, Anal. Chem. 24 (1952) 318.
[45] B. Nolin, R.N. Jones, J. Am. Chem. Soc. 75 (1953) 5626.
[46] N.B. Colthup, J. Opt. Soc. Am. 40 (1950) 397.
[47] R.S. Rasmussen, J. Chem. Phys. 16 (1948) 712.
[48] R.A. Meiklejohn, R.J. Meyer, S.M. Aronovic, H.A. Schuette, V.W. Meloch, Anal. Chem. 29 (1957) 329.
[49] R. Mecke, K. Noack, Spectrochim. Acta 12 (1958) 391.
[50] R. Barlet, M. Montagne, P. Arnaud, Spectrochim. Acta A: Mol. Spectrosc. A 25 (1969) 1081.
[51] E.G. Hoffmann, Annalen Der Chemie-Justus Liebig, 6181958 276.
[52] J.C. Lavalley, N. Sheppard, Spectrochim. Acta A: Mol. Spectrosc. 28 (1972) 2091.
[53] N.B. Colthup, L.H. Daly, S.E. Wiberley, Introduction to Infrared and Raman Spectroscopy, third ed. Academic Press, San Diego and London, 1990.
[54] M.L. Laury, M.J. Carlson, A.K. Wilson, J. Comput. Chem. 33 (2012) 2380.
[55] K. Christmann, G. Ertl, O. Schober, Surf. Sci. 40 (1973) 61.
[56] T.E. Felter, S.M. Foiles, M.S. Daw, R.H. Stulen, Surf. Sci. Lett. 171 (1986) L379.
[57] W. Eberhardt, S.G. Louie, E.W. Plummer, Phys. Rev. B 28 (1983) 465.
[58] Stein, S. E. In NIST Chemistry WebBook, NIST Standard Reference Database Number 69; Mallard, P. J. L. A. W. G., Ed.; National Institute of Standards and Technology: Gaithersburg MD, (August 1, 2014).